JOURNAL OF GEOPHYSICAL RESEARCH, VOL. 101, NO. C7, PAGES 16,515–16,531, JULY 15, 1996

Kinematic and dynamic evolution of deep water breaking waves

Owen M. Griffin,[1] Rodney D. Peltzer, and Henry T. Wang

Remote Sensing Division, Naval Research Laboratory, Washington, D.C.

William W. Schultz

Mechanical Engineering and Applied Mechanics Department, University of Michigan, Ann Arbor, MI

Abstract. Experiments were performed to exploit the dispersive properties of unsteady surface waves and to induce breaking by using a modified chirp pulse technique to focus the wave energy at a specific location in the Naval Research Laboratory deep water wave channel. The experiments have resulted in a highly resolved archive of breaking events ranging from wave steepening and incipient breaking to spilling and to plunging. The potential energy density, the crest front steepness, the horizontal asymmetry, and other geometric properties of an incipient breaker vary only within a moderate band about their mean values over the extent of these experiments. Thus the properties of an incipient unsteady breaker are well defined. The application of the phase-time or Hilbert transform method to the data set provides new insights into the local properties of the unsteady wave breaking. Recently, spectral and piecewise-linear algorithms for two-dimensional potential flow were developed and used by *Schultz et al.* [1994] to compare the onset of breaking for several methods of energy input to the unsteady wave system. The computations show that steep plunging waves occur when energy input rates are large. The various energy input methods exhibit similar breaking trends in the limit as the energy input rate becomes small in that incipient spilling breakers form when the potential energy is approximately 52 to 54% of the energy for the most energetic Stokes wave, with the formation of a singularity immediately before the crest.

Introduction

The physical complexities of wave breaking in deep water are widely recognized but still are not well understood after many years of study. Breaking waves are generally classified into two types: plunging, in which the forward face of the breaker overturns violently into the slope of the preceding trough; and spilling, in which the breaking and whitecapping develop more gently from an instability near the wave crest. The fluid dynamics of deep water breaking, especially the outstanding theoretical issues and new measurement approaches, were assessed most recently by *Longuet-Higgins* [1988] and by *Banner and Peregrine* [1993]. A related symposium evaluated the current state of knowledge for all aspects of wave breaking in order to stimulate further research in critical areas [*Banner and Grimshaw*, 1992].

Breaking waves are universally present over the ocean surface, and they play important roles in both the microwave and acoustic scattering processes at the surface [*Kerman*, 1988; *Melville et al.*, 1988]. An interesting study of the physical processes associated with microwave backscattering from wind-generated waves up to the onset of breaking was performed recently by *Ebuchi et al.* [1993].

The observation of highly localized, large backscatter events of short duration (sea spikes) in the surface radar signature at small grazing angles of a few degrees is attributed to the presence of steep and breaking waves [*Wetzel*, 1990; *Trizna et al.*, 1991]. Similar scattering events at larger look-down angles away from grazing have been described by *Jessup et al.* [1991a, b]. There is some controversy and considerable discussion among specialists over the scattering mechanisms and conditions that produce the spike-like features. However, the geometry of the wave near the crest but prior to the onset of visible breaking appears to play a leading role in the scattering process [*Loewen and Melville*, 1991; *Sletten and Savtchenko*, 1996].

Bright regions on the sea surface caused by breaking waves appear in many visual observations and synthetic aperture radar (SAR) images of surface ship wakes which have been remotely sensed from air and space over the past 20 years [*Munk et al.*, 1987; *Reed et al.*, 1990; *Griffin et al.*, 1992].

Wave breaking associated with wave steepness in the absence of wind is the topic of this paper. However, there are certain similarities when wind is included, and these are briefly discussed in the next section. Much of the prior research on wave breaking has been devoted to studying steady and regular monochromatic wave trains. In the present study we are interested in the more realistic behavior of unsteady wave groups or packets.

[1]Deceased September 29, 1995.

Paper number 96JC00281.
0148-0227/96/96JC-00281$09.00

Background

The fundamental experiments for studying two-dimensional wave breaking (apart from wind-generated waves which are discussed briefly later) fall into three main categories: (1) the focusing of essentially two-dimensional waves in the lateral direction [*Van Dorn and Pazan*, 1975; *Ramberg et al.*, 1985; *Ramberg and Griffin*, 1987]; (2) the towing of a submerged object, such as a hydrofoil to produce steady breakers [*Duncan*, 1981, 1983]; and (3) the focusing of variable-length waves from a modulated or chirped wave maker to produce unsteady breakers [*Dommermuth et al.*, 1988; *Duncan et al.*, 1987; *Rapp and Melville*, 1990; *Peltzer et al.*, 1993; *Duncan et al.*, 1994; *Sletten and Savtchenko*, 1996] or the overturning of an irregular wave train [*Ochi and Tsai*, 1983; *Bonmarin*, 1989] to produce unsteady breakers.

One of the most extensive laboratory studies of unsteady deep water breaking thus far is the work of *Rapp and Melville* [1990]. The dispersive character of the deep water waves was used to focus a wave packet and to generate a single unsteady breaking event at a controlled location in the wave channel. Losses of excess momentum and energy flux during breaking within a wave group ranged from 10% for spilling breakers to 25% for plunging breakers. Rapp and Melville found that the growth rate of the waves prior to breaking was an important factor in predicting breaking. This had been found previously by *Van Dorn and Pazan* [1975] and, to a lesser extent, by *Ramberg et al.* [1985] and *Ramberg and Griffin* [1987] in their convergent channel experiments.

Su et al. [1982] give an excellent review and laboratory study of the growth of the nonlinear instabilities of steep gravity wave trains up to the onset of breaking. Experiments were performed in both a wave channel and a wave basin. Regular two-dimensional wave trains with initial steepnesses of $a_o k_o$ from 0.25 to 0.33, where a is amptitude and k is wave number, evolved to three-dimensional spilling breakers after a period of strong nonlinear interactions and then subsequently to less steep two-dimensional wave groups. Typical average steepnesses of the spilling breakers were approximately $ak \sim 0.42$. The breaking waves exhibited steep crest fronts and asymmetries.

Several of these experimental studies propose a wave-breaking criterion based on peak-to-peak (crest-to-trough) wave height. However, the validity of a standard or global criterion has been questioned [*Melville and Rapp*, 1988], in part because peak-to-peak wave heights vary significantly during breaking and often decrease just before the onset of breaking. Clearly, no breaking criterion can be simple and precise. *Schultz et al.* [1994] opt for a simple potential energy criterion in the hope that it can be more universally applied, although experimentally or computationally determined criteria are a function of many parameters. Extensive discussions of breaking criteria based on wave height are given by *Ochi and Tsai* [1983], *Huang et al.* [1992], *Xu et al.* [1986], *Bonmarin* [1989], and *Dawson et al.* [1993]. Global breaking criteria based on the wave crest acceleration are discussed by *Longuet-Higgins* [1985] and *Srokosz* [1986]. Precise experimental determination of the onset of breaking is difficult without detailed velocity measurements at the crest, e.g., *Van Dorn and Pazan* [1975] and *Melville and Rapp* [1988], which are quite limited in number and are difficult to obtain as well.

Computational studies of breaking waves usually form the waves by applying a point pressure disturbance [*Longuet-Higgins and Cokelet*, 1976, 1978] or obtain breaking conditions simply from having sufficiently energetic initial conditions [*Vinje and Brevig*, 1981]. While many algorithms have been developed that simulate breaking waves, *Schultz et al.* [1994] were first to systematically study incipient breaking. For example, wave breaking caused by a modulated wave maker has been verified computationally by *Dommermuth et al.* [1988], but these computations were so expensive that only one experimental event was verified. *Wang et al.* [1994] computed the evolution of unsteady waves to breaking over a large computational domain which they call their numerical wave tank. They found good qualitative agreement near breaking between the computed nonlinear wave profiles and breaking waves photographed by *Ramberg et al.* [1985], *Ramberg and Griffin* [1987], and *Bonmarin* [1989]. In general, computations before *Schultz et al.* tend to show plunging waves instead of the more commonly observed spilling breakers on the ocean surface.

Schultz et al. [1994] computationally examined the steepening and breaking of deep water waves generated by the experimental methods cited above. Only spatially periodic computations were used, so an ad hoc energy input term was deduced for the convergent wave channel. Although the periodic boundary conditions precluded studying the wave maker problem, the effect of wave modulation was examined using a larger computational region (more than one primary wavelength) as in the work by *Dold and Peregrine* [1986]. The effect of beach reflections was modeled by putting a small standing wave component in the initial conditions. To crudely model waves produced by submerged hydrofoils, a periodic array of simple submerged dipoles was used.

There are difficulties in interpreting the differences caused by the computational spatial periodicity as compared to the temporal periodicity which is common to many experiments. Also, experiments continue after breaking occurs, while the time-marching computations must stop at the first occurrence of breaking unless an ad hoc condition models the turbulence and air entrainment. *Schultz et al.* [1994] show that accurate spectral computations break down sooner, indicating the possible formation of a singularity and evidence of the failure of potential theory before the forward wave crest becomes vertical.

Recent measurements of the limiting wave height at breaking for paddle-generated waves at laboratory conditions are summarized in Table 1 and Figure 1. Laboratory measurements of the limiting heights of regular deep water waves by *Ochi and Tsai* [1983], *Ramberg and Griffin* [1987], and *Bonmarin* [1989] have shown that the onset of breaking occurs at heights which are appreciably less than Stokes' theoretical limiting value, as shown. The present Naval Research Laboratory (NRL) experiments, as well as those of *Bonmarin* [1989], *Rapp and Melville* [1990], and *Dawson et al.* [1993], show that the onset of breaking in unsteady wave groups or packets occurs at still lower local wave heights. The reduced wave heights at breaking from these experiments are represented in Table 1 by the corresponding values of the breaking coefficient or effective steepness σ that are listed there. A mean value of $\sigma = 0.019$ was obtained by *Xu et al.* [1986] from their wave channel experiments for the so-called dominant form of wind-induced incipient breaking. The

Table 1. Mean Values of the Deep-Water Wave Breaking Coefficient $\sigma = H/gT^2$

Reference	Legend	Breaker Type	
	Figure 1	Plunging	Spilling
Stokes (theoretical limit)		--	0.027
Ochi and Tsai [1983]	diamonds	0.020	--
Ramberg and Griffin [1987]	triangles	--	0.021 (1)
Bonmarin [1989]	half-solid squares	0.022 (2)	0.021 (4)
		0.020 (3)	0.020 (5)
Rapp and Melville [1990]	box area	--	0.017 - 0.021 (4)
Present NRL experiments	"	0.018 - 0.021 (2)	0.017 - 0.018 (4)

Numbers in parentheses are defined as follows: 1. spilling and lightly plunging; 2. typical plunging; 3. plunging; 4. typical spilling; and 5. spilling (from *Bonmarin* [1989]). NRL is Naval Research Laboratory.

results of these experiments performed by *Xu et al.* are given in Figure 2, which shows that the data scatter approximately +/- 15% about the line with a slope σ = 0.019.

NRL Experiments

Experiments were performed in the NRL deep water wave channel to exploit the dispersive properties of unsteady surface waves in order to produce an extensive matrix of breaking events over a representative range of controlled wave packet properties. These experiments were performed in the channel 30 m long, 1.2 m wide, and 1 m deep, shown in Figure 3. The channel as shown here is configured to perform not only the breaking wave experiments discussed in this paper, but also wind stress and surface radar backscatter measurements as well. Packets of waves were generated by a hydraulically actuated paddle driven under computer control. The method of wave packet generation employed in these experiments represents a further refinement of the chirp pulse generation technique for focusing the wave energy at a desired location in the channel [*Clay and Medwin*, 1977; *Rapp and Melville*, 1990].

Two examples of the wave generator voltage inputs or control signals for the experiments are shown in Figure 4.

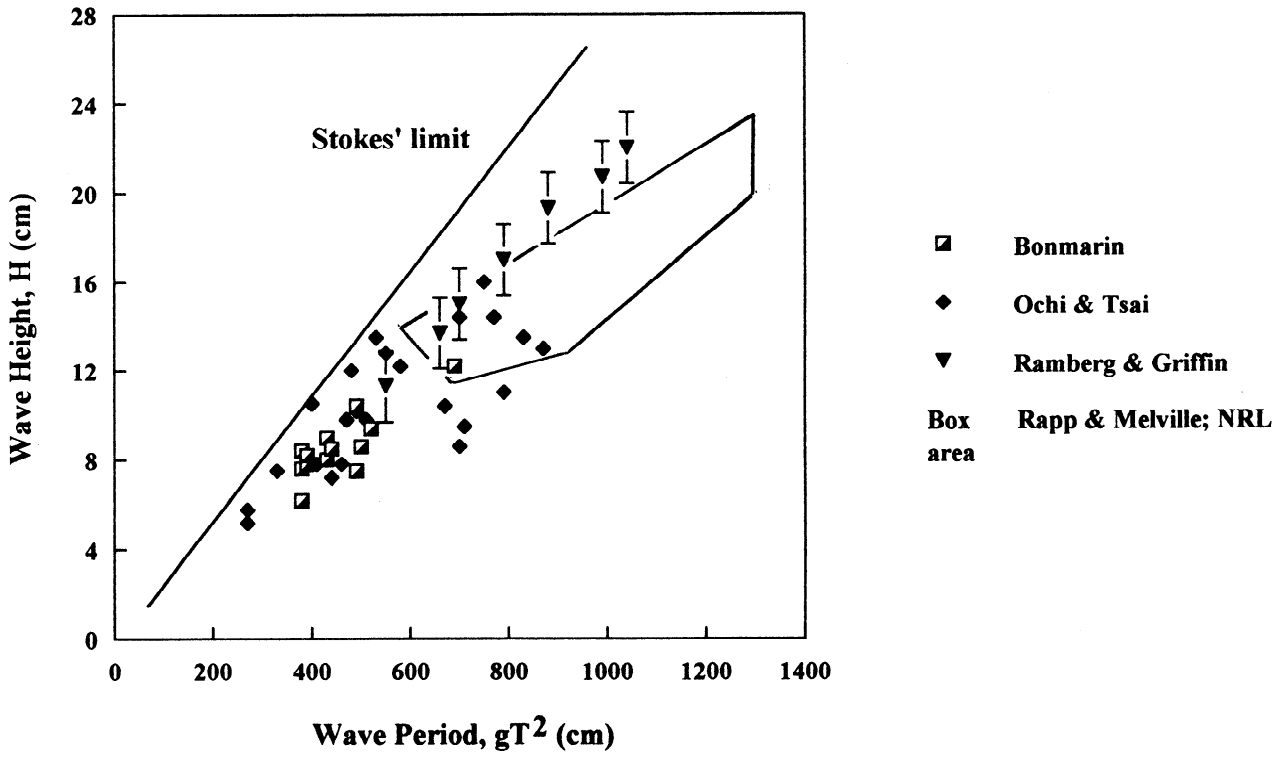

Figure 1. Laboratory measurements of the limiting height H of paddle-generated deep water waves as a function of the period parameter gT^2. The legend for the experimental data is given in Table 1.

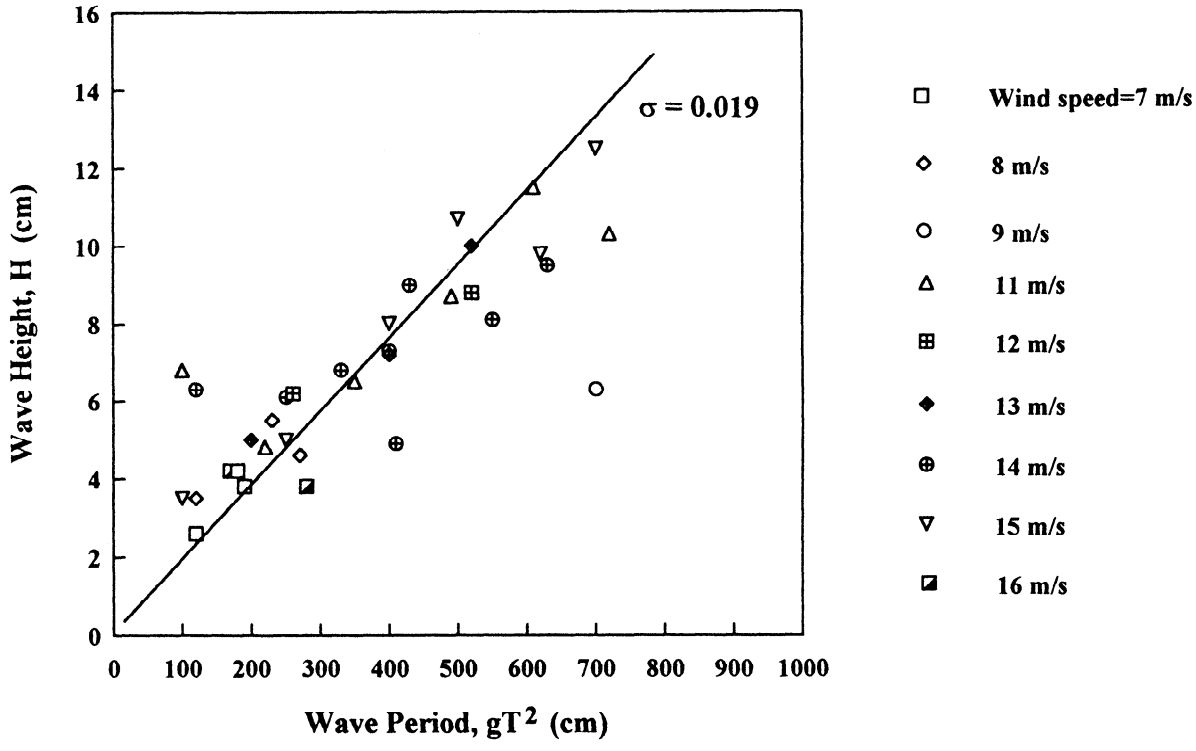

Figure 2. Laboratory measurements of the limiting height H of wind-generated deep water waves as a function of the period parameter gT^2 [data from *Xu et al.* 1980]. Wind speeds range from 8 to 16 m/s in the plotted data. The straight line, best fit to the data has a slope of $\sigma = 0.019$.

The wave packet consists of $M = 32$ sinusoidal components of small amplitude and evenly spaced in frequency. Only the amplitude and duration of the wave packet of 12 waves with a Gaussian envelope were varied during the present experiments. The overall periods of the initial input wave packets varied from 13 to 16 s, corresponding to frequency factors (FF) ranging from FF42 to FF34, as shown in Figure 4. The maximum initial amplitude of the largest wave within any packet formed in the wave channel by driving the hydraulically actuated paddle with these voltage input signals was varied from 0.09 to 0.25 m in order to span a suitable range of breaking conditions. The wave generator voltage input examples shown in Figure 4 are generic to all the packet signals for a given FF series, since the signal amplitudes are normalized with respect to the maximum value of the signal for a given packet. A typical arrangement of the

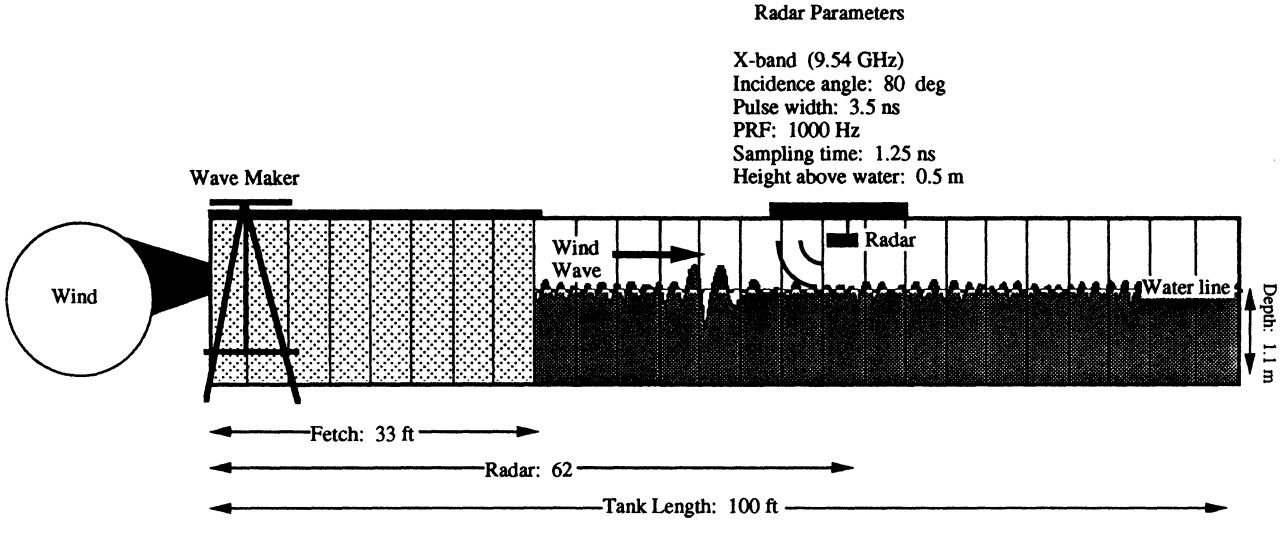

Figure 3. Layout of the Naval Research Laboratory (NRL) deep water wave channel (from F. Askari and T. Donato, Naval Research Laboratory, private communication, 1994). The channel in the configuration shown was also set up to measure radar scattering from the breaking waves.

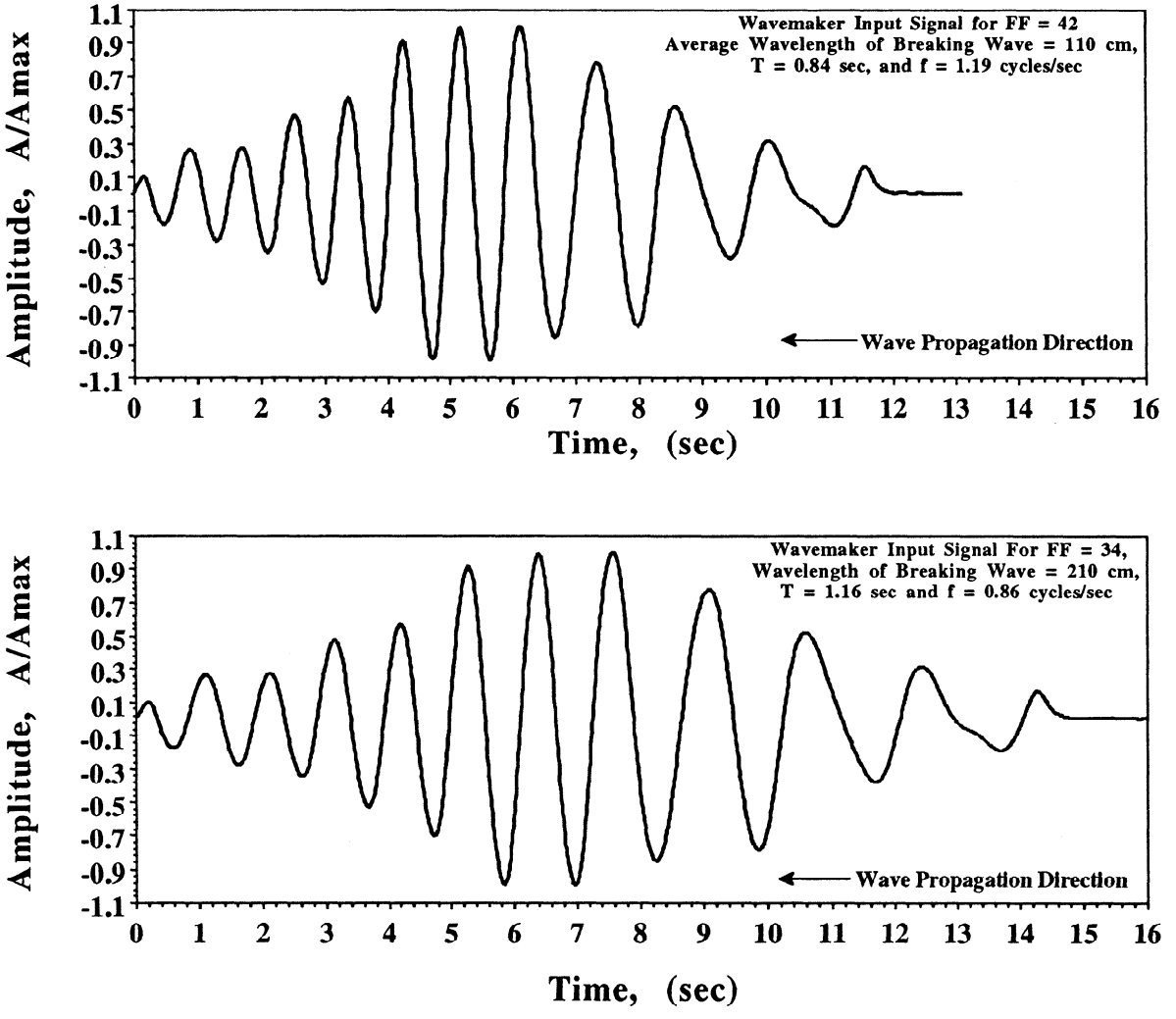

Figure 4. Wave generator control signals for the chirp pulse wave packet employed in the NRL experiments. The two examples shown are for the packets (top) FF42 and (bottom) FF34.

wave gauges in the channel is sketched in Figure 5a. This chirped pulse technique also has been used by *Duncan et al.* [1994] to generate precisely controlled spilling breakers.

The breaking conditions ranged from incipient breaking or gently spilling to intermediate (whitecapping) and to fully plunging (overturning). The temporal histories of the waves were measured using an array of seven Churchill conductivity gauges with their associated signal conditioning modules. The gauges were calibrated before and after each experimental run by displacing each one vertically over a series of known displacements and recording the results. The waves' spatial evolution was recorded with a high-resolution (SVHS) video camera and recording system. A grid with 2.5 x 2.5 cm spacing was attached to the Plexiglas walls of the channel to facilitate interpretation of the video recordings.

Wave Evolution

The evolution of a typical wave packet in the NRL wave channel is plotted in Figure 5b for an initial condition which produces an incipient breaker. Each of the time histories plotted is the average of three independent realizations. The initial steepness (at gauge G1) of the wave which eventually breaks within the packet is $a_0 k_0 = 0.238$. The local amplitude a_0 of the eventually breaking wave at this gauge is taken as half the wave height H, a good approximation as shown in Figure 5b, and the wave number is $k_0 = 2\pi / l$, the local wavelength of the eventually breaking wave. The value of l (in centimeters) is obtained from the dispersion relation between wavelength and period T,

$$l = \frac{gT^2}{2\pi} = 155.97T^2 \qquad (1)$$

where T is estimated by the zero downcrossing method for the largest wave crest and preceding trough of the wave at gauge G1 corresponding to the eventual incipient spilling wave. The reference wave number k_0 is defined as the value at gauge G1 pertaining to the wave of lowest steepness (a spilling wave) in each packet series. The frequency factor FF34 refers to the packet (see Figure 4) with the nominally largest period of the breaking wave of about 1.2 s. The evolution of the initially Gaussian packet to a short, sharply peaked breaking wave

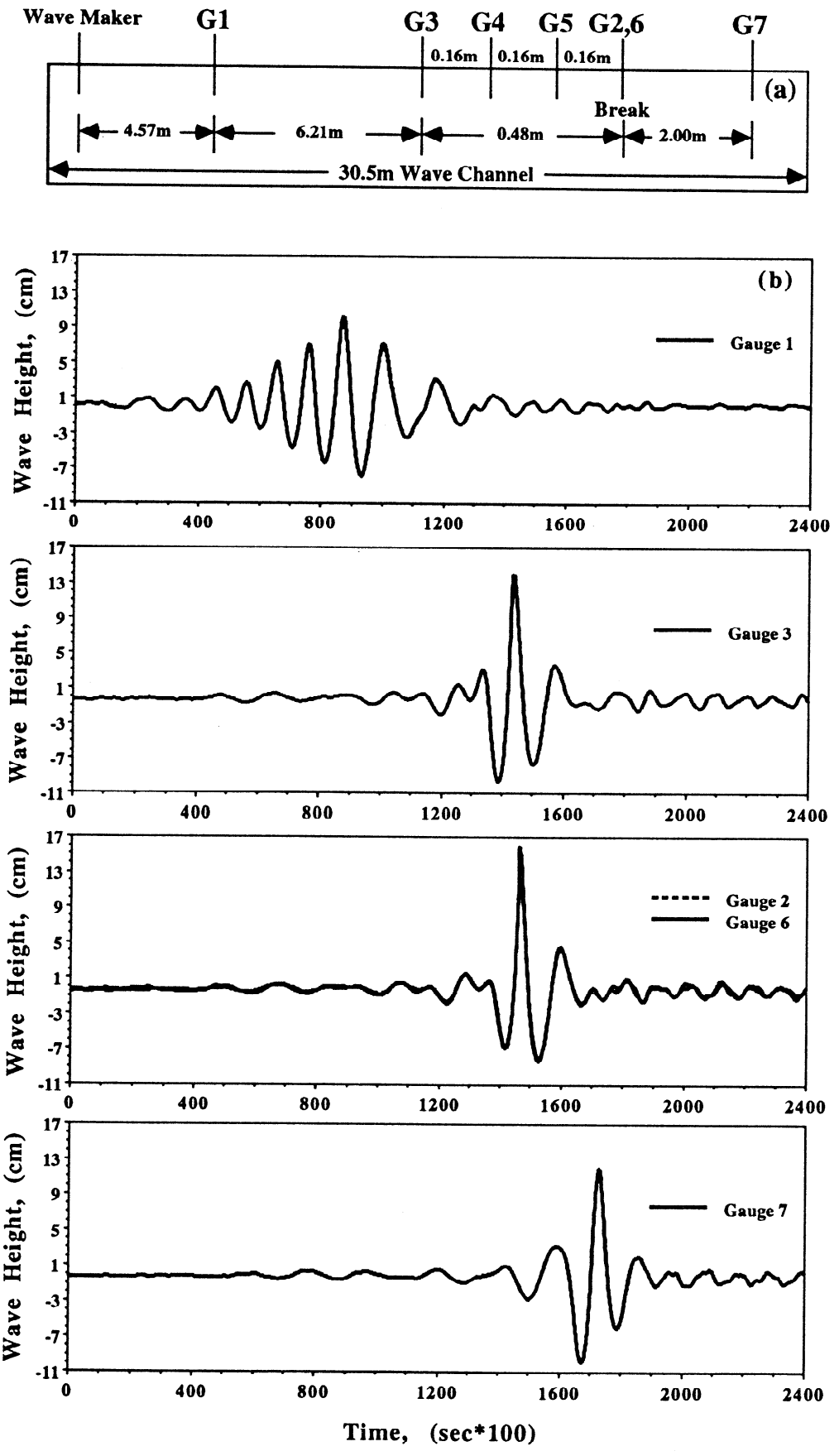

Figure 5. (a) A line diagram of the relative locations of the wave gauges in the NRL wave channel. (b) Evolution of a wave packet measurement time history in the channel for initial wave paddle conditions which produce an incipient breaker. Frequency factor is of the wave packet FF34 (see Figure 4 and Table 2).

train is evident as the downstream location of breaking (gauges G2, G6 at $k_o x$ = 20.54) is reached. The local wavelength for the particular wave under study in the packet at these gauges was obtained in the same manner as for gauge G1. All of the events investigated in these experiments were limited to the first occurrence of breaking in the packet, prior to any secondary breaking that followed.

The change in form of the steepest wave in the packet near breaking can be observed in the sequence of wave profiles shown in Figure 6, again for the condition given by FF34. The profiles are individual frames that are digitized from the video recordings. The round wave still resembles the profile of a steep, symmetric Stokes wave. The increases in the steepness and asymmetry of the crest region which accompany the progression in severity of breaking are observable as the process evolves from a steep but nonbreaking wave just before the incipient stage, to a spilling breaker, then to an intermediate level of breaking, and finally, to a fully plunging or overturning breaker. The onset of rippling and very light spilling at the crest appears at the incipient stage of breaking. Then a region of increasing agitation and flow complexity near the crest is formed as the breaking progresses through the intermediate stages toward full plunging or overturning. It is this progression which is discussed here in terms of the geometry or steepness and energy properties of the wave packet.

Potential Energy

The potential energy per unit of surface area or the density v, averaged locally over the wavelength l, is

$$v = \frac{1}{l}\left(\frac{\rho g}{2}\int_0^l \eta^2 dx\right) \tag{2}$$

where ρ is the water density, g is the gravitational acceleration, η is the wave amplitude, and x is the direction of wave propagation. This equation can be expressed in the nondimensional form

$$epl = \frac{2vk^2}{\rho g} = \frac{k^2}{N}\sum_{i=1}^{N}\eta_i^2 \tag{3}$$

where the η_i are the N individual data points in the local wave gauge record, and k is the local wave number at the gauge.

The spatial evolution of the potential energy density, averaged over a wavelength (period), is plotted in Figure 7a for the same wave packet (FF34). The potential energies span

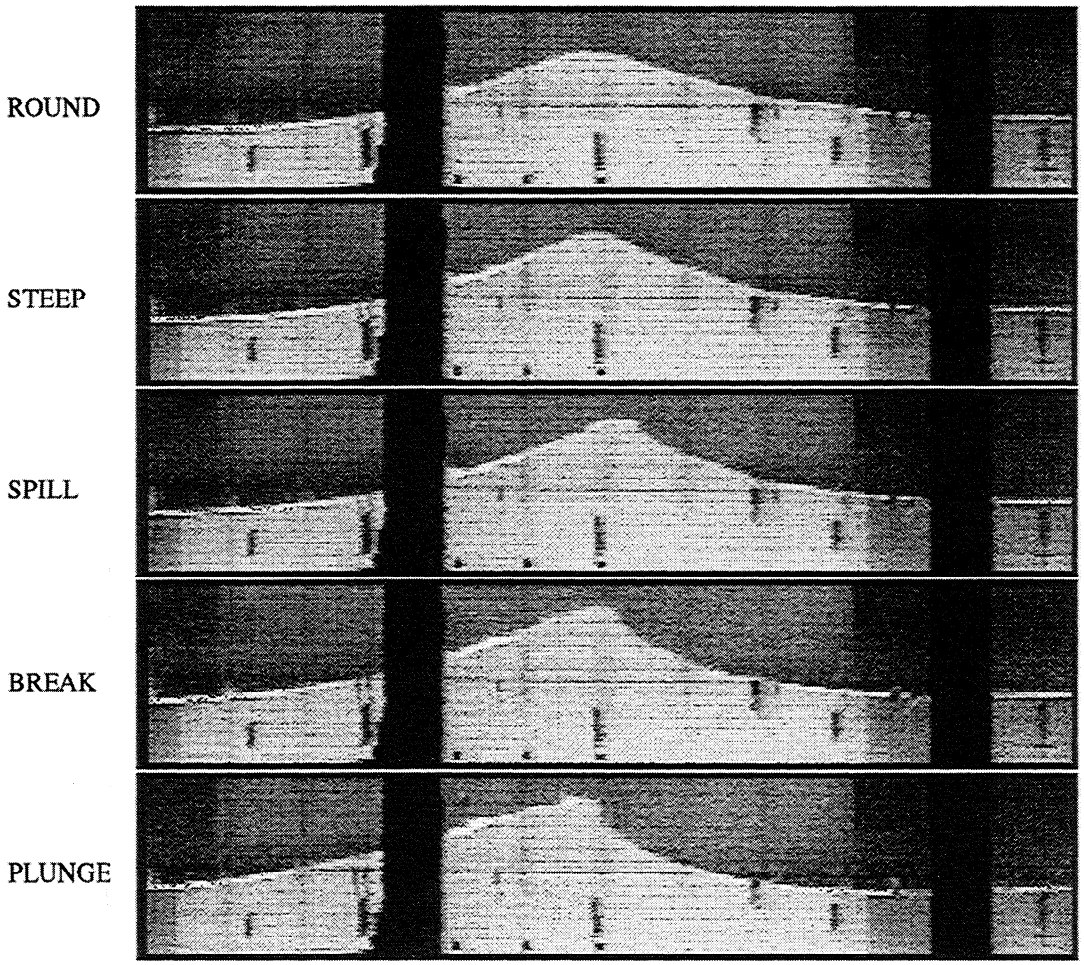

Figure 6. Still video frames of a sequence of laboratory deep water wave profiles ranging in levels of steepness and breaking from round, to steep (near incipient), to spilling, to intermediate, and to plunging. The frequency parameter of the wave packet is FF34.

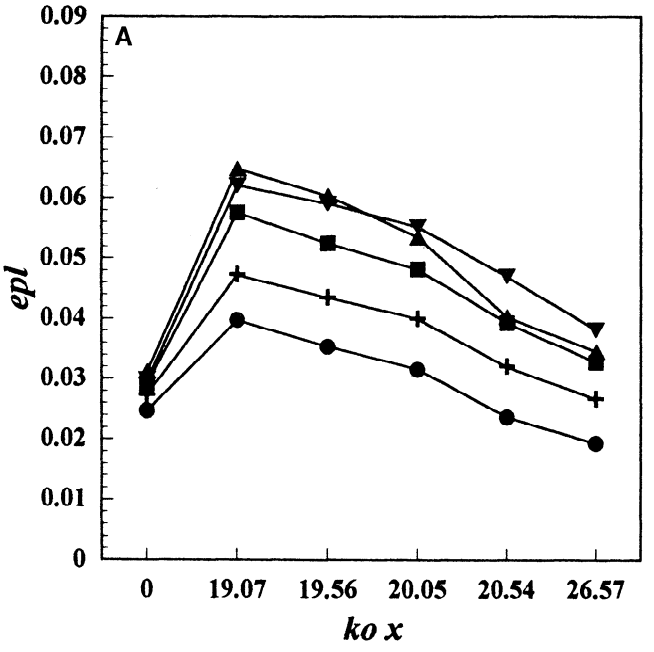

Figure 7a. Spatial evolution of the average potential energy per unit surface area, scaled by $2k^2$, with distance along the wave channel, scaled by the wavenumber k_0 (at gauge G1). The frequency factor shown is of the wave packet FF34. The wave breaking takes place at k_0x = 20.54. Initial steepness a_0k_0 is 0.224 (circles), 0.238 (pluses), 0.247 (squares), 0.255 (triangles), and 0.248 (inverted triangles).

a range of initial conditions from steep, but nonbreaking (a_0k_0 = 0.224), to incipient breaking or spilling (a_0k_0 = 0.238), to intermediate (a_0k_0 = 0.247), and to fully plunging (a_0k_0 = 0.248 and 0.255). The initial steepnesses for the packets FF37 and FF42 in Figures 7b and 7c are somewhat greater. This variation primarily is due to the range of the initial steepnesses a_0k_0 at gauge G1, which could be controlled only to a limited extent. This was because the first gauge G1 was at a fixed physical location relative to the wave generator, whereas gauges G2 to G7 were moved as the location of breaking within the wave channel changed for the different packets with different values of a_0k_0.

Two key features of the breaking event are observed in these experiments. First, the potential energy at breaking increases as the progression in severity proceeds from gently spilling to fully plunging and overturning; and as the wave packet evolves along the channel, the spatial rate of change of the potential energy varies markedly with the severity of the breaking. The latter effect corresponds directly to the transformation of potential energy to kinetic energy and vice versa as the level of the breaking changes and as the initial conditions of the wave packet are changed. Note that gauge G1 is relatively far upstream of the breaking region, with $k_0\Delta x \sim 19$ ($\Delta x \sim 3\lambda_0$) between gauges G1 and G3 for series FF34 and $k_0\Delta x \sim 9$ ($\Delta x \sim 1.4\lambda_0$) for series FF42. In the breaking region the wave gauges are closely spaced, with $\Delta x \sim 0.23\lambda_0$ for FF34 and $\Delta x \sim 0.56\lambda_0$ for FF42 between gauge G3 and gauges G2 and G6. The distance between wave gauges is only a small fraction of a wavelength and so it is reasonable to assume that the measured potential energy density is constant or, at most, slowly varying between them.

For packet FF34 there is an overall decrease in potential energy *epl* as the packet travels from gauge G3 (k_0x = 19.07) toward the onset of breaking at gauges G2 and G6 (k_0x = 20.54). This decrease in potential energy prior to breaking over 0.48 m in along-channel distance accompanies a corresponding increase in kinetic energy, while the total energy is assumed here to remain constant except for small losses to boundary friction, etc., in the finite-area wave

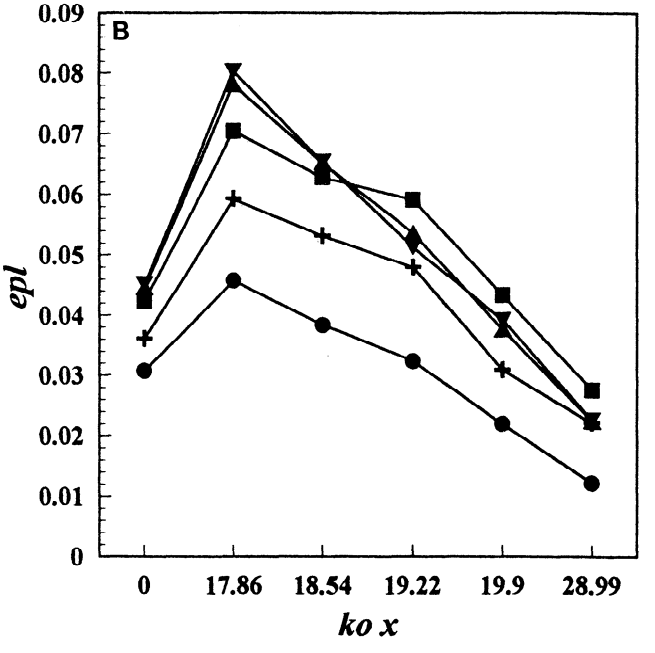

Figure 7b. Same as Figure 7a, but for frequency factor FF37 with wave breaking at k_0x = 19.90. Initial steepness a_0k_0 is 0.251 (circles), 0.273 (pluses), 0.294 (squares), 0.304 (triangles), and 0.306 (inverted triangles).

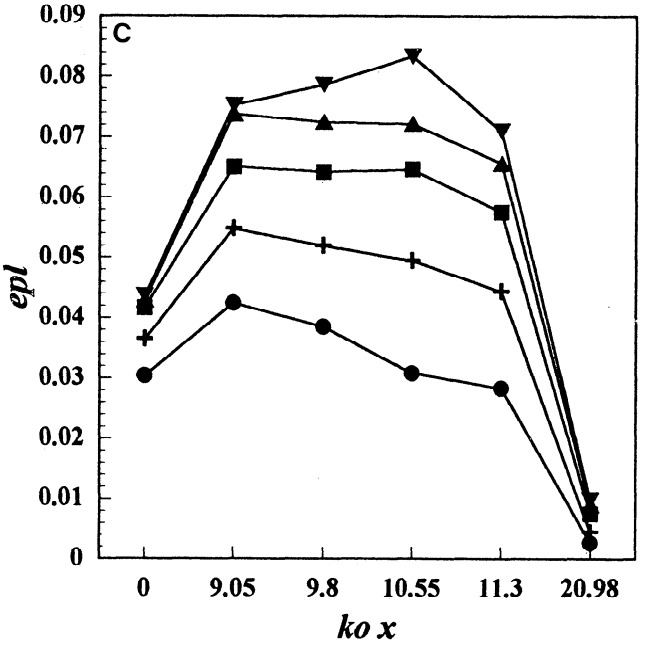

Figure 7c. Same as Figure 7a, but for frequency factor FF42 with wave breaking at k_0x = 11.30. Initial steepness a_0k_0 is 0.249 (circles), 0.279 (pluses), 0.294 (squares), 0.298 (triangles), and 0.302 (inverted triangles).

channel. *Rapp and Melville* [1990] showed that such losses are minimal by comparison to the total energy of a similar packet. Much the same pattern of behavior is observed for packet FF37.

Packet FF42 with the smallest breaking wave period (see Figure 4) exhibits a different evolutionary history as shown in Figure 7c. The incipient breaking packet with $a_o k_o = 0.279$ shows only a very small change in potential energy as $k_o x$ increases from 9.05 to 11.3 (gauge G3 to gauges G2 and G6). The potential energies of the intermediate and lightly plunging packets with $a_o k_o = 0.294$ and 0.298 initially remain nearly constant and only decrease over the short distance from $k_o x = 10.55$ (gauge G5) to 11.3 (gauges G2 and G6). The potential energy of the packet which evolves to a fully plunging event first increases up to $k_o x = 10.55$, then decreases. Thus the evolving histories of the various breaking waves are dependent on the initial properties of the packet in terms of frequency content and initial amplitude or steepness.

The potential energies of an unsteady incipient breaker as computed by *Schultz et al.* [1994] and measured in these NRL experiments are approximately half (52 to 54%) the potential energy of the highest symmetric Stokes wave as computed by *Cokelet* [1977]. It was not possible in the present experiments to measure the kinetic energy of the waves. Schultz et al. showed that the total energy of an inviscid numerical simulation of the unsteady waves up to breaking is 49 to 52% of that for the limiting Stokes wave and that the kinetic energy is slightly greater than the potential energy at breaking. It is reasonable to suppose that this partition of the energy in the wave applies as well to the present experiments.

Typical potential energies of the individual waves that break within the packet are *epl* = 0.0319 (spilling) and *epl* = 0.0469 (plunging) for FF34 and *epl* = 0.0443 and 0.0709, respectively, under the same nominal conditions for FF42. Only relative (local/initial) measurements of the evolution of the potential energy or momentum flux along the channel were made by *Melville and Rapp* [1985] and *Rapp and Melville* [1990]. To the extent that comparisons are possible, their results are qualitatively similar to our measurements of *epl* that are plotted here in Figures 7a - 7c. Approximately 75 to 90% of the total potential energy is concentrated in the crest region at breaking, with the proportion of the crest potential energy becoming consistently smaller for plunging breakers than for spilling breakers.

Wave Asymmetry and Steepness

Several geometric properties which characterize the wave asymmetry and steepness have been identified by *Kjeldsen and Myrhaug* [1978], *Bonmarin* [1989], and *Kjeldsen* [1990] as important and unique indicators of the evolution of a wave to breaking. The degree of asymmetry in the crest is expressed by horizontal and vertical asymmetry factors suggested by Bonmarin and Kjeldsen, i.e., μ and λ, and the steepness is expressed at the front and rear of the wave crest, i.e., ε and δ as defined in Figure 8. The crest front steepness ε, the ratio of the crest amplitude y_{max} to the distance F_1 from the crest to the previous zero level crossing, arguably is the most important of the four cited there.

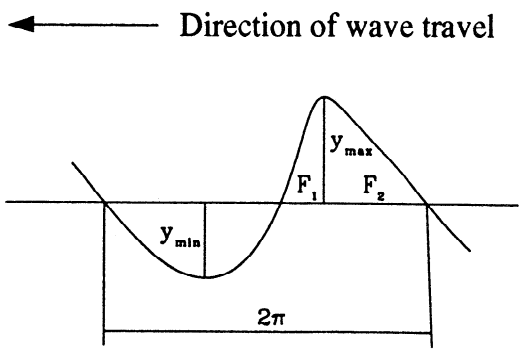

Horizontal Asymmetry Factor	$\mu = y_{max} / (y_{max} - y_{min})$
Vertical Asymmetry Factor	$\lambda = F_2 / F_1$
Crest Front Steepness	$\varepsilon = y_{max} / F_1$
Crest Rear Steepness	$\delta = y_{max} / F_2$

Figure 8. Definition of the asymmetry and steepness properties of a steep, nonlinear wave. The wavelength is chosen equal to 2π, for convenience, in this sketch, in following the convention of *Schultz et al.* [1994].

The relevance of these parameters toward characterizing a breaking wave has been recognized by the International Association for Hydraulic Research since 1986, and *Kjeldsen* [1996] has shown that they are applicable at full ocean scales as well as at laboratory scales for plunging breakers. Conversely, from their analysis of the results from an extensive North Sea field experiment, *Holthuijsen and Herbers* [1986] found that not wave height (steepness), crest front steepness, nor horizontal asymmetry could be used with confidence to discriminate spilling breakers from nonbreaking steep waves in their data set. The steepness and asymmetry of the waves in the field invariably were smaller by a considerable margin than those observed in laboratory experiments.

The crest front steepnesses measured with the wave gauge array for series FF34 and FF42 are plotted in Figures 9a and 9b. The initial values of $a_o k_o$ for each breaking wave packet are the same as in Figures 7a - 7c. The packet with the smallest initial steepness corresponds to a steep but nonbreaking wave condition. This is followed by an incipient or spilling breaker, an intermediate breaker, and two plunging breakers as before. The measured ε in these experiments are in excellent agreement with the limited results of *Bonmarin* [1989] and *Rapp and Melville* [1990] for incipient spilling and plunging breakers. But the present experiments, as summarized in Figures 9a and 9b, give a more detailed history of the crest region evolution than any previous experiment. The maximum crest front steepnesses for a plunging breaker in Figures 9a and 9b are $\varepsilon = 0.56$ at FF34 and $\varepsilon = 0.60$ at FF42. For the NRL data set overall the largest plunging steepness is $\varepsilon = 0.62$ for the wave packet denoted by FF37. Unlike the potential energies shown in Figures 7a - 7c the behavior of ε for a given type of wave shows little variation between series FF34 and FF42.

The vertical asymmetry $\lambda = F_2/F_1$ provides another measure of the deformation of the crest region as breaking is approached. The evolution of λ for series FF34 and FF42 is plotted in Figures 10a and 10b, again, the initial steepness conditions are as described above. All of the waves are

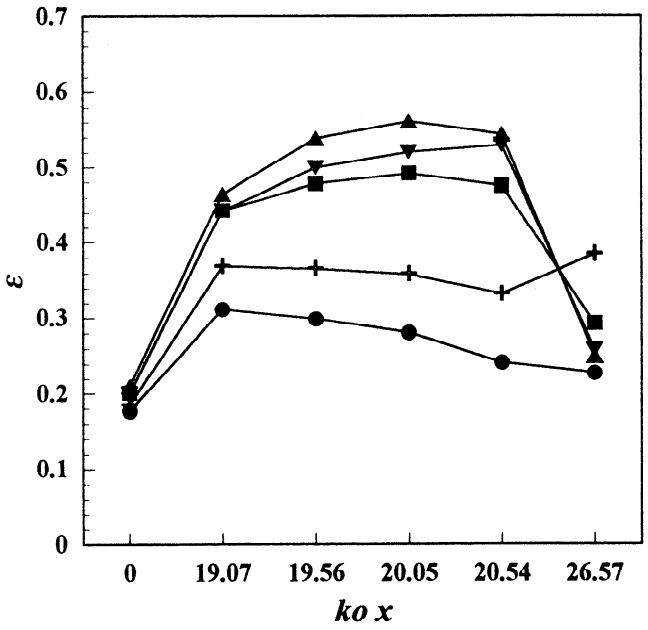

Figure 9a. Spatial evolution of the crest front steepness ε with distance along the wave channel. The frequency factor of the wave packet is FF34 with the wave breaking taking place at $k_o x = 20.54$. Initial steepness $a_o k_o$ is 0.224 (circles), 0.238 (pluses), 0.247 (squares), 0.255 (triangles), and 0.248 (inverted triangles).

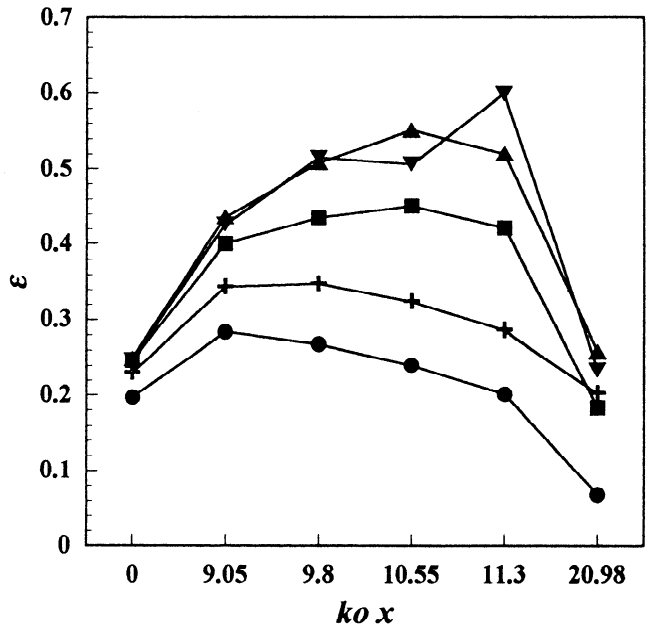

Figure 9b. Same as Figure 9a, but for frequency factor FF42 with wave breaking at $k_o x = 11.30$. Initial steepness $a_o k_o$ is 0.249 (circles), 0.279 (pluses), 0.294 (squares), 0.298 (triangles), and 0.302 (inverted triangles).

essentially symmetric about the crest or $\lambda \sim 1$ at the first wave gauge. For the nonbreaking wave and the spilling (incipient) breaker the vertical asymmetry varies only moderately and decreases slightly as the location of breaking in the channel (at gauges G2 and G6) is approached. As the intermediate stage of breaking is approached, the wave profile about the crest becomes decidedly asymmetrical. When the plunging condition is reached, the profile becomes still more asymmetric with the ratio $F_2/F_1 = 2$ just before breaking for the series FF34. The horizontal asymmetry μ, the ratio of the crest amplitude to the full wave height, changes only slightly as the breaking evolves from the incipient stage toward fully

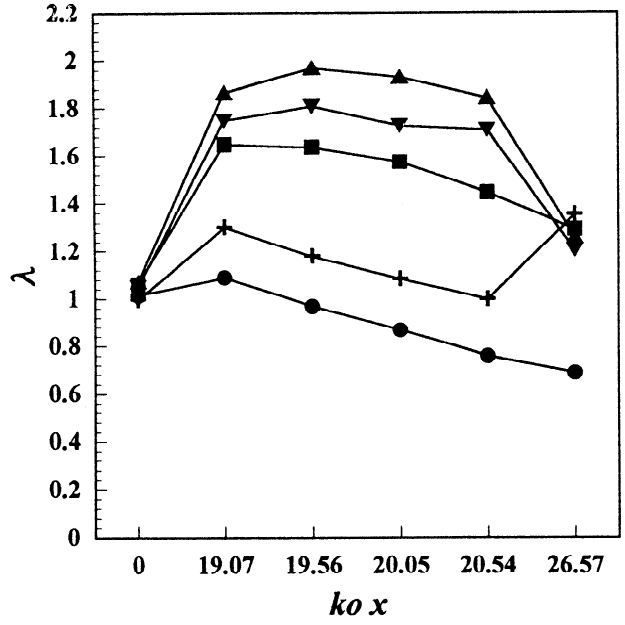

Figure 10a. Spatial evolution of the vertical asymmetry λ with distance along the wave channel. The frequency factor of the wave packet is FF34 with the wave breaking taking place at $k_o x = 20.54$. Initial steepness $a_o k_o$ is 0.224 (circles), 0.238 (pluses), 0.247 (squares), 0.255 (triangles), and 0.248 (inverted triangles).

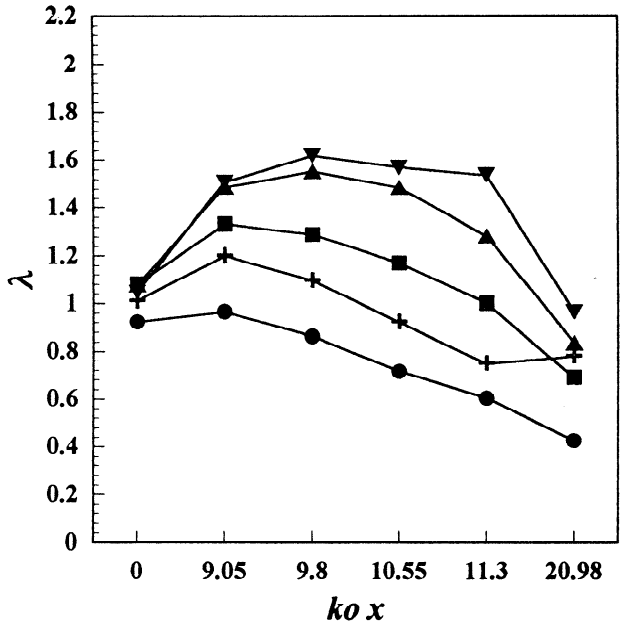

Figure 10b. Same as Figure 10a, but for frequency factor FF42 with wave breaking at $k_o x = 11.30$. Initial steepness $a_o k_o$ is 0.249 (circles), 0.279 (pluses), 0.294 (squares), 0.298 (triangles), and 0.302 (inverted triangles).

plunging ($0.72 < \mu < 0.80$) for these NRL experiments. Most of the increase in the wave steepness just prior to breaking results from the reduced length of the region forward of the crest, i.e., the crest front. *Duncan et al.* [1987] quote an average value of $\mu = 0.75$ at the breaking point for both spilling and plunging breakers.

Much the same progression in asymmetry as the crest region increases in steepness can be observed from the video images in Figure 6. Both the round and steep waves are quite symmetric about the crest, while the spilling breaker gives some evidence of the onset of asymmetry. As the plunging stage of breaking is reached, the vertical asymmetry from the images qualitatively matches well with the comparable wave gauge measurements. The results in Figures 10a and 10b indicate that the geometry of the wave evolution toward breaking depends on the amplitude and frequency makeup of the wave packets as denoted by FF34 and FF42. The other wave packet series show this same dependence as well.

For these NRL experiments the vertical asymmetry λ ranged from about 0.9 to 1.8. *Longuet-Higgins and Cokelet* [1978] computed a value $\lambda = 1.83$ for a plunging breaker. From his wave packet experiments, *Kjeldsen* [1990] found that $0.9 < \lambda < 2.2$, while *Bonmarin* [1989] measured the range of $1.2 < \lambda < 2.1$. *Duncan et al.* [1987] found that λ varied between 1.3 and 1.7 at breaking, for spilling and plunging breakers, respectively.

Analysis of Unsteady Breaking

For the analysis of a nonstationary, localized phenomenon, such as wave breaking, it is of interest to use techniques other than the traditional, global Fourier transform. This transform is most appropriate for signals which are periodic and stationary, but it is unsuitable for analyzing transient phenomena such as the unsteady evolution of a wave packet up to breaking. Instead, the Hilbert transform or the phase-time method, as it sometimes is called [*Huang et al.*, 1992; *Long*, 1996], is here used to obtain a local analysis of the time-varying amplitude and frequency behavior of the breaking wave. While a breaking wave's geometric properties have been studied before as in this paper, the evolution of the amplitude and frequency content of the wave near breaking has not been studied before by this method of analysis.

The Hilbert transform $\tilde{y}(t)$ is a convolution of the wave signal $y(t)$ and the time windowing function $1/(\pi t)$ over the entire duration T of the signal. In conjunction with the original signal the Hilbert transform is used to give the instantaneous envelope signal $A(t)$, the phase signal $\theta(t)$, and the frequency $f_0(t)$, as follows

$$A(t) = \left[y^2(t) + \tilde{y}^2(t)\right]^{1/2}$$
$$\theta(t) = \tan^{-1}\left[\tilde{y}(t)/y(t)\right] \quad (4)$$
$$f_0(t) = \frac{1}{2\pi}\left[d\theta(t)/dt\right]$$

The Hilbert transforms of the measured wave data were obtained by using the function contained in the MATLAB software package. Each of the time histories is an average of three independent realizations, and a total of seven wave packets were analyzed. These represent a subset of the 10 cases considered for the FF34 and FF42 series in Figures 9a and 9b, omitting the intermediate wave in both series and the less severe plunging wave of FF34. The notation for these cases is as follows: the first two numbers give the FF series, the next two letters give the type of wave (ro = round = nonbreaking, sp = spilling = incipient breaking, pl = plunging = severe breaking), and the last two numbers give the strength of the voltage applied to the wave generators.

Figure 11 shows a time history of the wave elevation for these seven cases consisting of 501 data points corresponding to 2.5 s on either side of the maximum elevation as measured at gauge G2 (where $t\text{-}t_{max} = 0$). It should be emphasized that the Hilbert transforms were obtained for the entire measured time history which ranged from a minimum of 1441 points to a maximum of 2811 points. The choice of the time axis clearly shows the differences in general amplitudes and periods between different waves in a given series and between the two series. Figure 11 also generally confirms a wave period of approximately 1.16 s for FF34 and 0.84 s for FF42 as in Figure 4.

A somewhat different and more concise view is obtained by plotting the instantaneous Hilbert amplitude $A(t)$ for the seven cases as shown in Figure 12. In addition to the differences between individual waves and series of waves, Figure 12 clearly shows the asymmetry between the front and

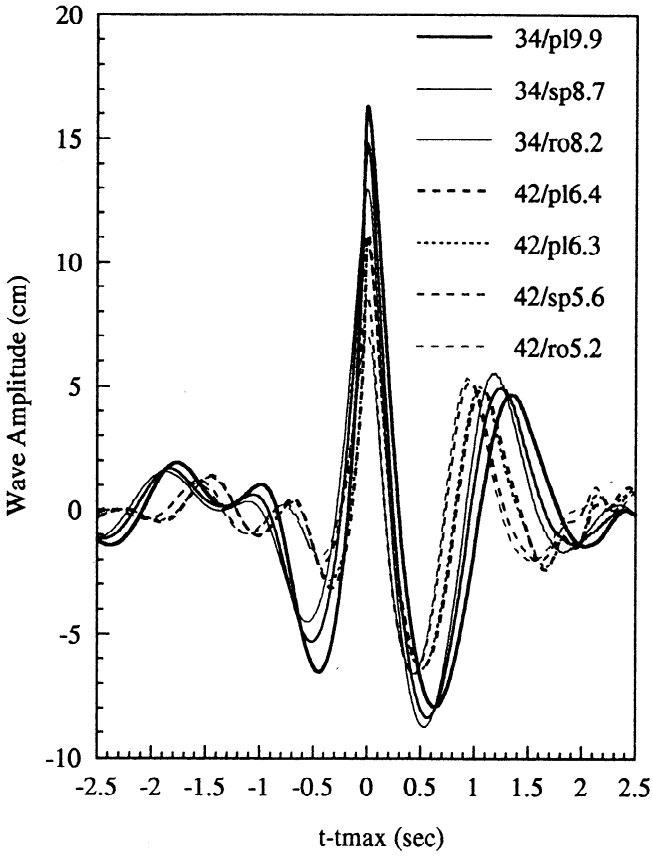

Figure 11. The time history of the local wave elevation at gauge G2, the location of breaking. Abbreviations are pl, plunging; sp, spilling; and ro, round.

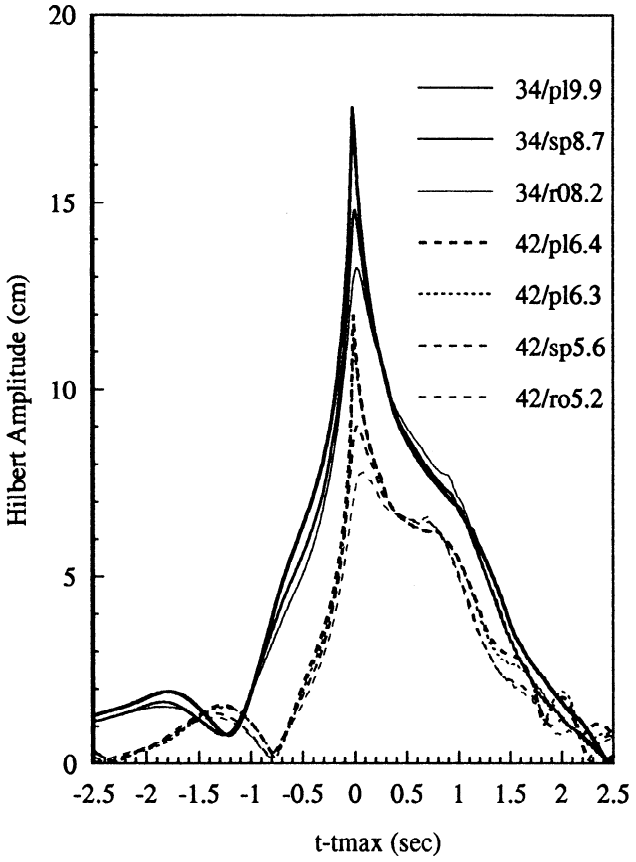

Figure 12. The time history of the Hilbert amplitude at gauge G2.

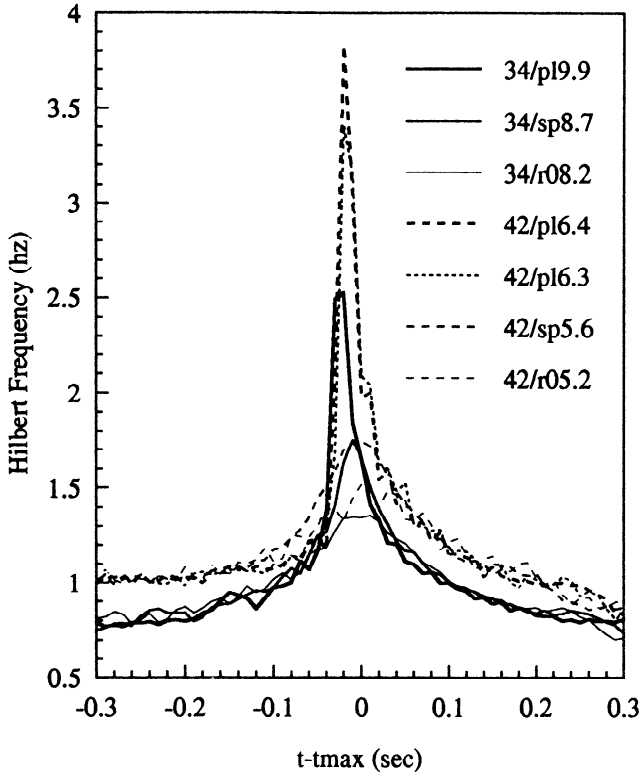

Figure 13. The time history of the Hilbert frequency at gauge G2.

rear faces of the wave. The asymmetry of the wave form as determined by this method is more pronounced for the steeper FF42 waves.

In order to provide a new and more precise view of the wave breaking process, the time variations of the instantaneous Hilbert frequencies f_o are shown in Figures 13, 14, and 15. Figure 13 shows f_o for the seven cases in the narrow region $-0.3 < t\text{-}t_{max} < 0.3$. This more closely focuses on the local region of wave breaking. The most dramatic variation in frequency occurs in the region $-0.1 < t\text{-}t_{max} < 0.1$, with a more gentle variation outside of this region. The maximum frequencies are approximately 1.35 and 1.5 Hz for the round waves, 1.75 Hz for both spilling waves, and 2.5, 3.4, 3.8 Hz for the three plunging waves. Figure 13 also shows more clearly the difference between the two plunging waves for FF42.

Figure 14 shows a more global view of the evolution of the breaking wave process. Figure 14 shows the values of f_o for gauges G3, G4, G5, and G2 in the interval $-0.5 < t\text{-}t_{max} < 0.5$ for the plunging (omitting the least severe case for FF42), spilling, and round waves for FF34 and FF42. The frequency profiles show that the evolution process is qualitatively similar for corresponding waves in both packet series. The frequency behavior is nearly constant with gauge location for the round waves and shows slight growth for the two spilling waves and sharp growth for the two plunging waves, with the FF42 case showing the most severe growth. The trend is similar to the variation of crest front steepness with gauge location shown in Figs. 9a and 9b.

It is also of interest to investigate the energy content of a segment of the wave around the breaking point as a function of frequency. Since the phenomenon is nonstationary, the shape of the function depends on the length of record which is chosen. Here the length is chosen for the interval $-5.5 < t\text{-}t_{max} < 5.5$, which corresponds approximately to the interval of significant wave activity at gauge G2 as shown in Figure 5. A Hilbert energy density spectrum $E_H(f_{oi})$ can be constructed numerically by summing the Hilbert energy $A^2\ dt/2$ contained in each frequency bin centered around f_{oi}, $i = 1,2,\ldots,N_{B-1},N_B$ (N_B is the number of bins), and dividing the result by the width of the frequency bin. The choice of N_B is governed by the conflicting requirements of choosing as large a value as possible to get a detailed definition of the shape of E_H and the opposing need to minimize the number of bins to obtain stable energy estimates.

Figure 15 shows E_H for $N_B = 14$, with 12 of the bins equally spaced between 0.1 and 2.5 Hz, and the remaining two bins accounting for $f_o < 0.1$ and $f_o > 2.5$ Hz, respectively. Taking the typical number of samples in a bin (N_S), equal to 1100/14 = 79, the normalized standard error of the energy estimate in a typical bin is approximately given by the expression $\sigma = 1/(N_S)^{1/2} = 0.11$. Within a given run series, E_H is highest for the plunging waves and lowest for the round waves at frequencies less than approximately 1.0 Hz. The round waves and steep waves have the highest energy at intermediate frequencies. Only the plunging waves have significant energy for frequencies greater than 1.8 Hz.

Additional Comparisons

The potential energy *epl*, the crest front steepness ε, and the horizontal asymmetry μ measured at the incipient stage

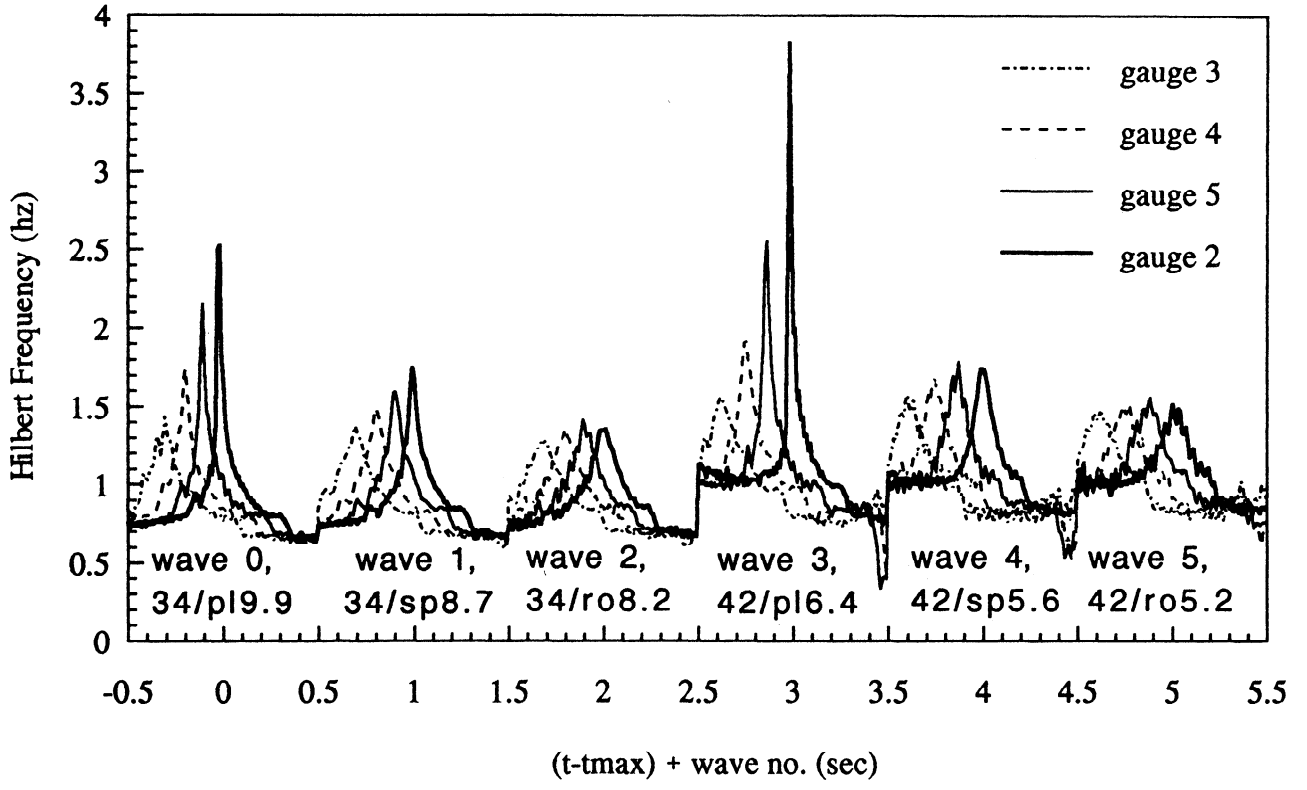

Figure 14. The evolution of the Hilbert frequency at gauges G3, G4, G5, and G2. The gauge locations are given in Figure 4a.

of breaking and beyond are summarized in Figures 16, 17, and 18, respectively, for several experimental runs which cover the range in Table 2. The incipient breaking properties are the first cases plotted for each of nine runs in these figures. Four wave packets which range from incipient to plunging are shown for runs 34, 37, 39, 41, and 42. There is a distinct increase in the potential energy and crest front steepness as the breaking levels increase from incipient or spilling, to intermediate, and to plunging. The dependence on initial steepness is evident from the results in Figures 16 and 17.

The horizontal asymmetry, the crest front steepness, and the average potential energy density of an incipent breaker vary only moderately about their mean values (μ = 0.772, ε = 0.299, *epl* = 0.0346] for the nine wave packet series listed in Table 2. The present experiments are in good agreement with the recent numerical simulations of the same breaker properties μ, ε and *epl* by *Schultz et al.* [1994], as well as the range of ε at incipient breaking from the experiments of *Rapp and Melville* [1990]. *Kjeldsen* [1990] cites a value of μ = 0.77 at the onset of breaking in a wave group from his laboratory experiments, again in good agreement with the present experiments. *Bonmarin* [1989] found that μ ranged from 0.69 to 0.77 for spilling versus plunging breakers. For the NRL experiments shown in Figure 18 the horizontal asymmetry ranged from μ = 0.72 to 0.80, depending on the severity of the breaking. These properties plus others such as the vertical asymmetry λ locally define the incipient breaking condition for an unsteady wave. *Longuet-Higgins* [1996] and *Duncan et al.* [1996] have proposed that the incipient stage of breaking is related to the appearance of an instability at the crest region as it steepens and becomes more asymmetric.

Table 3 gives the average of the crest front steepness ε, and the RMS of the average of the incipient breaking waves from Table 2. The RMS value proves to be a more reliable and consistent criterion than a steepness criterion for breaking inception [*Schultz et al.*, 1994] This is especially beneficial for the wave packet criterion because the RMS wave height

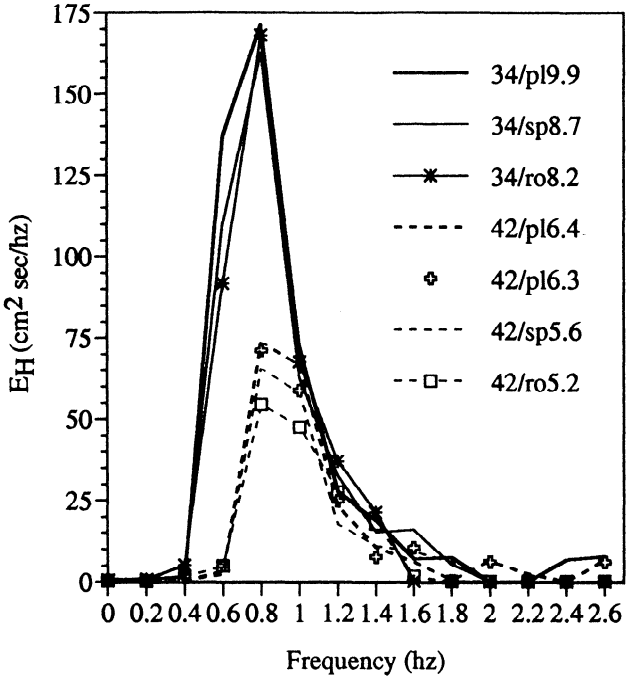

Figure 15. The Hilbert energy density spectrum at gauge G2.

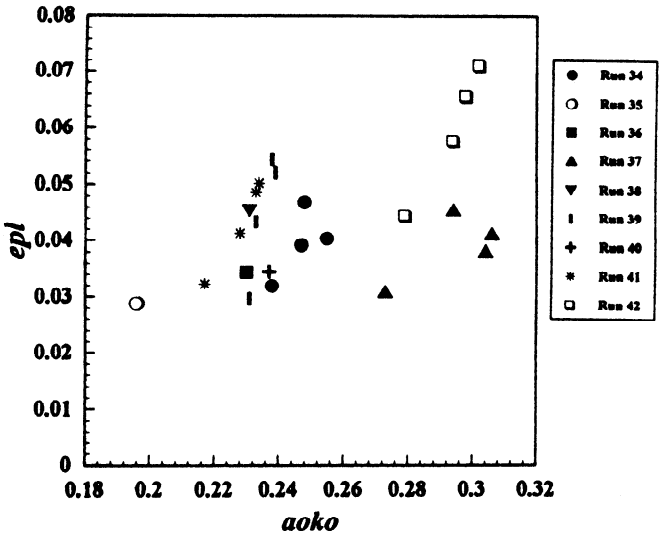

Figure 16. The potential energy *epl* at breaking, measured during nine wave channel run series (see Table 2), as a function of the initial wave packet steepness. Symbols for the data series are as follows: FF34 (solid circles), FF35 (open circles), FF36 (solid squares), FF37 (triangles), FF38 (inverted triangles), FF39 (vertical bars), FF40 (pluses), FF41 (stars), FF42 (open squares).

can be predicted more directly and accurately than the wave steepness from simple group velocity considerations. These are not spatially periodic waves, and so a measure of breaking inception not based on wavelength is desirable, especially when the number of waves in a packet changes instantaneously as in this NRL example. The potential energy per unit surface area appears more consistent than the steepness in this regard, but the potential energy or its RMS value in this example uses the local wavenumber measured at the breaking location (from the results in Table 2) for scaling purposes.

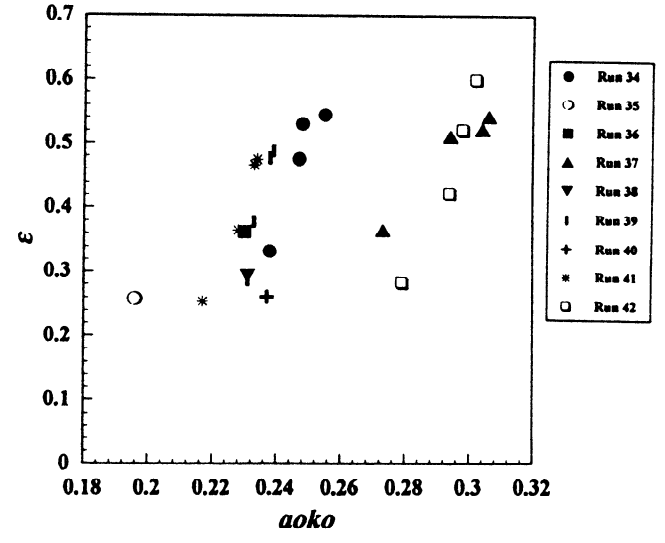

Figure 17. The crest front steepness ε at breaking, measured during nine wave channel run series, as a function of the initial wave packet steepness. Symbols are the same as Figure 16.

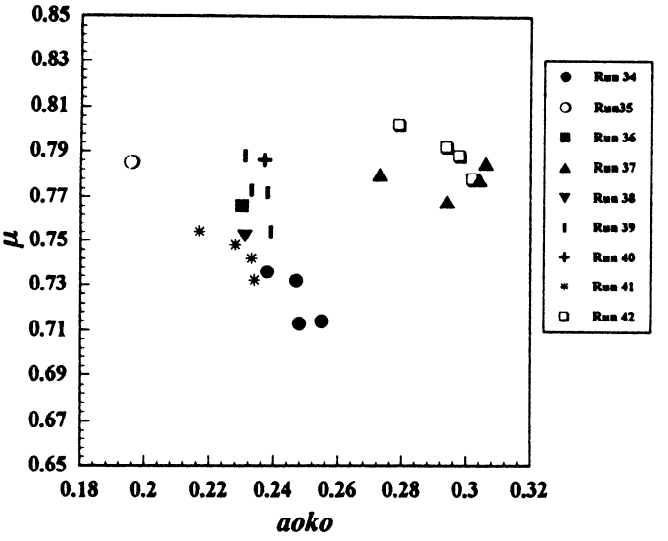

Figure 18. The horizontal asymmetry μ at breaking, measured during nine wave channel run series, as a function of the initial wave packet steepness. Symbols are the same as Figure 16.

Concluding Remarks

These NRL experiments show that the initiation of unsteady breaking in a deep water wave group or packet depends on the initial packet conditions. Likewise, the evolution of the breaking wave's potential energy and its crest steepness and asymmetry properties prior to breaking also are dependent on these conditions; but the potential energy density, the crest front steepness, and the horizontal asymmetry of an incipient spilling breaker vary only within a moderate band about their mean values over the extent of the experiments.

The recent computations of *Schultz et al.* [1994] show that the potential energy of surface gravity waves is a better measure of the onset of breaking for steep nonlinear waves than either the wave height or wave slope. The computed wave height or steepness appears to have more erratic variations in time than the potential energy.

There is some experimental evidence that the square root of the potential energy (the RMS wave height) is better than the peak-to-peak wave height (or steepness) criteria in predicting an incipient breaking event. This is indicated by a smaller percentage variation of individual wave channel breaking events as compared to an average measure of the breaking.

The experiments demonstrate that the onset of breaking in a finite group or packet of waves consistently occurs at amplitudes (steepnesses) much lower than those measured for a train of regular waves. Thus global wave steepness criteria for the onset of breaking cannot be applied in general, and their use should be approached with some caution. This point also was noted by *Xu et al.* [1986] from their study of laboratory wind-generated breaking and by *Rapp and Melville* [1990] from their earlier laboratory experiments with unsteady wave packets.

The onset of breaking depends on the energy input rate to the wave system, with the smallest values occurring when the energy input rate is small and spilling breakers are expected.

Table 2. Incipient Breaking of an Unsteady Wave Packet

Frequency Factors	Initial Steepness $a_o k_o$	Horizontal Asymmetry μ	Crest Front Steepness ε	Potential Energy *epl*
34/8.7	0.238	0.736	0.333	0.0328
35/8.2	0.196	0.785	0.257	0.0287
36/7.7	0.230	0.766	0.362	0.0344
37/7.4	0.273	0.780	0.365	0.0309
38/6.8	0.231	0.752	0.293	0.0454
39/6.4	0.231	0.788	0.286	0.0296
40/6.2	0.237	0.786	0.260	0.0344
41/5.8	0.217	0.753	0.253	0.0322
42/5.6	0.279	0.802	0.282	0.0430
Mean	0.237	0.772	0.299	0.0346
Experiment [a]	0.23 - 0.26	--	0.28 - 0.35	--
Comparison [b]	0.28	0.72	0.40	0.0382

[a] Values are from *Rapp and Melville* [1990], breaking wave packet (six measurements).
[b] Values are from *Schultz et al.* [1994], initially steep, uniform wave train.

A smooth transition to plunging breakers occurs (as conjectured by *Longuet-Higgins and Cokelet* 1976] for higher waves that can be formed by a larger energy input rate. The dependence on the energy input rate further explains the scatter of breaking criteria derived from earlier experiments.

The phase-time or Hilbert transform method provides a promising alternative to the traditional global Fourier transform for the analysis of nonstationary local phenomena, such as unsteady wave breaking. This method was applied to the results from the NRL wave channel experiments and gives a new perspective on the time-varying evolution of a wave packet towards breaking. The instantaneous Hilbert amplitude clearly focuses on the asymmetry between the front and rear faces of the wave and shows the pronounced asymmetry present in the steepest wave packets. The spatial evolution of the Hilbert frequency of the packet toward breaking in the wave channel shows nearly constant behavior for the steep but nonbreaking waves, slight growth for spilling breakers, and a progression to sharp growth for fully plunging breakers. The trend is similar to the variation in crest front steepness obtained directly from the array of wave gauges. These initial results using the Hilbert transform approach agree well with the more traditional measurements of the wave properties near breaking that also are employed in this study.

Kjeldsen [1990, 1996] proposed that the crest front steepness gives a unique geometrical measure of the wave evolution as breaking is approached at both laboratory and full ocean scales, and the results of the present experiments tend to bear this out for laboratory-scale waves. The crest front steepness may be the most important wave property from the standpoint of radar scattering. Both *Loewen and Melville* [1991] and *Sletten and Savtchenko* [1996] have observed that a large portion of the radar backscatter from the wave precedes the onset of visible breaking. Thus the geometric properties of the wave form just prior to breaking appear to dominate the scattering process. *Wetzel* [1990] also stresses the importance of some as yet undetermined properties of the local steepness geometry to the surface radar scattering. The present results tend to support these propositions, but further research is warranted.

Acknowledgments. The experiments were performed and analyzed with support from a basic research program in free surface fluid dynamics at the Naval Research Laboratory. The work at the University of Michigan was supported by the Ocean Engineering Division of the Office of Naval Research, and the Program in Ship Hydrodynamics at the University of Michigan was funded by a University Research Initiative of ONR. The authors are grateful to Farid Askari, Lewis Wetzel, Mark Sletten, and Timothy Donato of NRL for many helpful discussions on various aspects of radar scattering from breaking waves.

Table 3. Properties of Incipient Breaking Unsteady Wave Packets

	ε	RMS
Experimental mean	0.299	0.186
Experimental standard deviation (%)	13.8	7.6
Prediction by *Schultz et al.* [1994]	0.40	0.195
Prediction/experiment comparison, (%)	25	5

References

Banner, M.L., and R.H.J. Grimshaw (Eds.), *Breaking Waves*, Springer-Verlag, New York, 1992.

Banner, M.L., and D.H. Peregrine, Wave breaking in deep water, *Annu. Rev. Fluid Mech., 25*, 373-397, 1993.

Bonmarin, P., Geometric properties of deep water breaking waves, *J. Fluid Mech., 209*, 405-433, 1989.

Bonmarin, P., and A. Ramamonjiarisoa, Deformation to breaking of deep water gravity waves, *Exp. Fluids, 3*, 11-16, 1985.

Clay, C.S., and H. Medwin, *Acoustical Oceanography*, Wiley-Interscience, New York, 1977.

Cokelet, E.D., Steep gravity waves in water of arbitrary depth, *Phil. Trans. R. Soc. London A, 286*, 183-230, 1977.

Dawson, T.H., D.L. Kriebel, and L.A. Wallendorf, Breaking waves in laboratory-generated JONSWAP seas, *Applied Ocean Research, 15*, 85-93, 1993.

Dold, J.W., and D.H. Peregrine, Water-wave modulation, Rep. AM-86-03, School of Math., Univ. of Bristol, England, 1986.

Dommermuth, D.G., D.K. Yue, W.M. Lin, R.J. Rapp, E.S. Chan, and W.K. Melville, Deep-water plunging breakers: A comparison between potential theory and experiments, *J. Fluid Mech., 189*, 423-442, 1988.

Duncan, J.H., An experimental investigation of breaking waves produced by a towed hydrofoil, *Proc. R. Soc. London A, 377*, 331-348, 1981.

Duncan, J.H., The breaking and non-breaking wave resistance of a two-dimensional hydrofoil, *J. Fluid Mech., 126*, 507-520, 1983 .

Duncan, J.H., L.A. Wallendorf, and B. Johnson, An experimental investigation of the kinematics of breaking waves, *Rep. EW-7-87*, U.S. Nav. Acad., Annapolis, Md., 1987.

Duncan, J.H., V. Philomon, M. Behres, and J. Kimmel, The formation of spilling breaking water waves, *Phys. Fluids, 6*, 2558-2560, 1994.

Ebuchi, N., H. Kawamura, and Y. Toba, Physical processes of microwave backscattering from laboratory wind wave surfaces, *J. Geophys. Res. 98(C8)*, 14,669-14,681, 1993.

Griffin, O.M., R.D. Peltzer, A.M. Reed, and R.F. Beck, Remote sensing of surface ship wakes, *Nav. Eng. J., 104*, 245-258, 1992.

Holthuijsen, L.H., and T.H.C. Herbers, Statistics of waves observed as whitecaps in the open sea, *J. Phys. Oceanogr., 16*, 290-297, 1986.

Huang, N.E., S.R. Long, C.C. Tung, M.A. Donelan, Y. Yuan, and R.J. Lai, The local properties of ocean waves by the phase-time method, *Geophys. Res. Lett., 19(7)*, 685-688, 1992.

Jessup, A.T., W.K. Melville, and W.C. Keller, Breaking waves affecting microwave backscatter, 1, Detection and verification, *J. Geophys. Res., 96(C11)*, 20,547-20,559, 1991a.

Jessup, A.T., W.K. Melville, and W.C. Keller, Breaking waves affecting microwave backscatter, 2, Dependence on wind and wave conditions, *J. Geophys. Res. 96(C11)*, 20,561-20,269, 1991b.

Kerman, B.R. (Ed.), *Sea Surface Sound, Natural Mechanisms of Surface Generated Noise in the Ocean*, Kluwer Acad., Norwell, Mass., 1988.

Kjeldsen, S.P., Breaking waves, in *Water Wave Kinematics*, edited by A. Torum and O.T. Gudmestad, pp. 453-473, Kluwer Acad., Norwell, Mass., 1990.

Kjeldsen, S.P., The wave follower experiment, in *Proceedings of the Symposium on the Air-Sea Interface*, edited by M. Donelan, Kluwer Acad., Norwell, Mass, in press, 1996.

Kjeldsen, S.P., and D. Myrhaug, Kinematics and dynamics of breaking waves - Main report, *VHL report STF 60 A 78100*, Vassdrags-og Havnelabortoriet, Trondheim, Norway, 1978.

Loewen, M.R., and W.K. Melville, Microwave and acoustic radiation from breaking waves, *J. Fluid Mech., 224*, 601-623, 1991.

Long, S.R., The Hilbert spectrum, A new tool for non-steady time series analysis, *Proceedings of the Symposium on the Air-Sea Interface*, edited by M. Donelan, Kluwer Acad., Norwell, Mass., in press, 1996.

Longuet-Higgins, M.S., Accelerations in steep gravity waves, *J. Phys. Oceanog., 15*, 1570-1579, 1985.

Longuet-Higgins, M.S., Mechanisms of wave breaking in deep water, in *Sea Surface Sound*, edited by B.R. Kerman, pp. 1-30, Kluwer Acad., Norwell, Mass., 1988.

Longuet-Higgins, M.S., The crest instabilities of steep gravity waves, in *Proceedings of the Symposium on the Air-Sea Interface*, edited by M. Donelan, Kluwer Acad., Norwell, Mass., in press, 1996.

Longuet-Higgins, M.S., and E.D. Cokelet, The deformation of steep gravity waves on water, I, A numerical method of computation, *Proc. R. Soc. London A, 350*, 1-26, 1976.

Longuet-Higgins, M.S., and E.D. Cokelet, The deformation of steep gravity waves on water, II, Growth of normal mode instabilities, *Proc. R. Soc. London A, 364*, 1-28, 1978.

Melville, W.K., The instability and breaking of deep-water waves, *J. Fluid Mech., 115*, 165-185, 1982.

Melville, W.K., and R.J. Rapp, Momentum flux in breaking waves, *Nature, 317*, 514-516, 1985.

Melville, W.K., and R.J. Rapp, The surface velocity field in steep and breaking waves, *J. Fluid Mech., 189*, 1-22, 1988.

Melville, W.K., M.R. Loewen, F.C. Felizardo, A.T. Jessup, and M.J. Buckingham, Acoustic and microwave signatures of breaking waves, *Nature, 336*, 54-59, 1988.

Munk, W.H., P. Scully-Power, and F. Zachariasen, The Bakerian Lecture: 1986 ships from space, *Proc. R. Soc. London A, 412*, 231-254, 1987.

Ochi, M.K., and C.-H. Tsai, Prediction and occurrence of breaking waves in deep water, *J. Phys. Oceanogr., 13*, 2008-2019, 1983.

Peltzer, R.D., O.M. Griffin, and W.W. Schultz, Steepness and energy properties of deep water breaking wave packets, in *Proceedings of the Symposium on the Air-Sea Interface*, edited by M. Donelan, Kluwer Acad., Norwell, Mass., in press, 1996.

Ramberg, S.E., and O.M. Griffin, Laboratory studies of steep and breaking deep water waves, *J. Waterw. Port Coastal Ocean Div. Am. Soc. Civ. Eng., 113*, 493-506, 1987.

Ramberg, S.E., M.E. Barber, and O.M. Griffin, Laboratory studies of steep and breaking deep water waves in a convergent channel, *NRL Memo. Rep., 5610*, May 1985.

Rapp, R.J., and W.K. Melville, Laboratory measurements of deep-water breaking waves, *Philos. Trans. R. Soc. London A, 331*, 735-800, 1990.

Reed, A.M., R.F. Beck, O.M. Griffin, and R.D. Peltzer, Hydrodynamics of remotely sensed surface ship wakes, *SNAME Trans., 98*, 319-363, 1990.

Schultz, W.W., J. Huh, and O.M. Griffin, Potential energy in steep and breaking waves, *J. Fluid Mech., 278,* 201-228, 1994.

Sletten, M.A., and A. Savtchenko, Ultrawideband, polarimetric radar studies of breaking waves at low grazing angles, *Radio Sci., 31,* 181-192, 1996.

Srokosz, M.A., On the probability of wave breaking in deep water, *J. Phys. Oceanogr., 16,* 382-385, 1986 .

Su, M.-Y., M. Bergin, P. Marler, and R. Myrick, Experiments on nonlinear instabilities and evolution of steep gravity-wave trains, *J. Fluid Mech., 124,* 45-72, 1982.

Trizna, D.B., J.P. Hansen, P. Hwang, and J. Wu, Laboratory studies of radar sea spikes at low grazing angles, *J. Geophys. Res. 96(C7),* 12,529-12,537, 1991.

Van Dorn, W.G., and S.P. Pazan, Laboratory investigation of wave breaking, II, Deep water waves, *Rep. 75-21,* Scripps Inst. Oceanogr., La Jolla, Calif., 1975 .

Vinje, T., and P. Brevig, Numerical simulation of breaking waves, *Adv. Water Resour. 4* , 77-82, 1981.

Wang, P., Y. Yao, and M.P. Tulin, Wave group evolution, wave deformation and breaking: Simulations using *LONGTANK*, a numerical wave tank, *International J. Offshore and Polar Engineering, 4(3),* 200-205, 1994.

Wetzel, L.B., Electromagnetic scattering from the sea at low grazing angles, in *Surface Waves and Fluxes, Vol. 2,* edited by G.L. Geernaert and W.J. Plant, pp. 109-171, Kluwer Acad., Norwell, Mass., 1990.

Xu, D., P.A. Hwang, and J. Wu, Breaking of wind-generated waves, *J. Phys. Oceanogr., 16,* 2172-2178, 1986.

R. D. Peltzer (corresponding author) and H. T. Wang, Code 7261, Remote Sensing Division, Naval Research Laboratory, 4555 Overlook Ave. SW, Washington, DC 20375-5351 (email: peltzer@neptune.nrl.navy.mil)

W. W. Schultz, MEAM Department, 313 Auto Lab, 1231 Beal Ave, University of Michigan, Ann Arbor, MI 48109-2121

(Received February 1, 1995; revised January 22, 1996; accepted January 22, 1996.)